The RadioAstron Project: Measurements and Analysis of Basic Parameters of Space Telescope in Flight in 2011−2013

Yu. A. Kovalev[a], V. I. Vasil'kov[a], M. V. Popov[a], V. A. Soglasnov[a], P. A. Voitsik[a], M. M. Lisakov[a], A. M. Kut'kin[a], N. Ya. Nikolaev[a], N. A. Nizhel'skii[b], G. V. Zhekanis[b], and P. G. Tsybulev[b]

[a] *Astro Space Center, Lebedev Physical Institute, Moscow, 119991 Russia*
e-mail: ykovalev@asc.rssi.ru
[b] *Special Astrophysical Observatory, Russian Academy of Sciences, Nizhnii Arkhyz, Russia*
Received December 16, 2013

Abstract—The results of a large number of the antenna radiometric measurements at bands of 92, 18, 6.2, 1.35, and 1.7−1.2 cm are presented by the data of the standard telemetry system of the *Spektr-R* spacecraft. Both special sessions of calibration object observations in the mode of a single space radio telescope (SRT) operation and numerous observations of researched sources in the mode of the ground−space interferometer were used. The obtained results agree with the first results of Kardashev et al. (2013), i.e., within 10−15% at bands of 92, 18, and 6.2 cm and 20−25% at the band of 1.35 cm. In the main, the measurements for the eight subbands at wavelengths of 1.7−1.2 cm indicate a monotonic increase in the spectral system equivalent flux density (SEFD) of noise radiation with a frequency consistent with the calculated estimates for the discussed model. The sensitivity of the ground−space interferometer for the five subbands at wavelengths from 1.35 to 1.7 cm can be higher by a factor of 1.5, and for the three subbands from 1.35 to 1.2 cm lower by a factor of 1.5 than at the band of 1.35 cm. The SRT contribution to the interferometer sensitivity proportional to the square root of SEFD is close to the design one at the bands of 92 and 18 cm and decreases the design sensitivity approximately by a factor of 1.5 and 2 at the bands of 6.2 and 1.35 cm, respectively. These differences of implemented values from the design ones were not significantly affected the scientific program implementation.

DOI: 10.1134/S0010952514050074

INTRODUCTION

The description of the *Spektr-R* spacecraft, the space radio telescope (SRT), scientific equipment, and ground tests are given in [1−3]. The results of flight tests, the technique and the first results of the antenna measurements of the basic telescope parameters using the radio astronomy methods in the radiometric mode at the bands 92, 18, 6.2, and 1.35 cm are presented in [4−6] for the effective area, the noise temperature, the radiation pattern, pointing error at a source, etc.

In this paper, we report new results of periodic tests of the basic SRT parameters in flight obtained in 2011−2013. The antenna measurements are performed both in special sessions of observations of calibration astronomical objects and during the current sessions of scientific observations in the mode of the ground−space radio interferometer.

The results of the antenna measurements are first presented for eight subbands of the frequency band of 18−25 GHz using in the mode of multifrequency image synthesis in further operation with the radio interferometer. To calibrate these measurements over flux, besides the known extended primary calibration sources (Cassiopeia A, Cygnus A, Crab, Virgo A), several quasi-point for SRT strong variable extragalactic objects (3C 84, 3C 273, 3C 279) have also been used, the spectral radiation flux density of which were measured on close dates relative to known secondary calibrators on the RATAN-600 radio telescope of Special Astrophysical Observatory (Nizhnii Arkhyz, Russia) and the 100-m telescope of the Max Planck Institute for Radio Astronomy (Effelsberg, Germany).

1. MEASUREMENTS

The measurements of the antenna parameters are based on the relative measurements of spectral system equivalent flux density (SEFD) of the noise radiation F_{sys} [Jy] relative to astronomical calibrators. The equivalent noise temperature of the system (radio telescope) T_{sys} was measured relative to the antenna temperature and considered to be known for onboard noise generators (in degrees K) that belong to each scientific receiver.

The onboard scientific complex includes four radio astronomical superheterodyne receivers at bands of 92, 18, 6.2, and 1.35 cm. The receiver at the band of 1.35 cm also provides a signal that receives from eight switchable subbands at 1.7−1.2 cm by choosing one of the subbands with corresponding commands. Units of input low-noise amplifiers (LNAs) of receivers for all
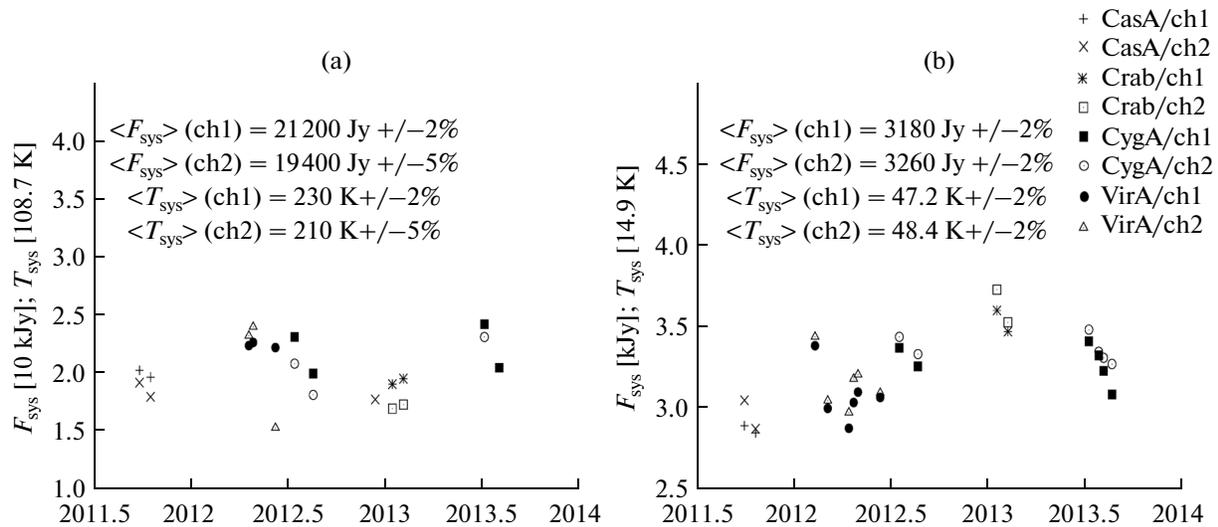
Fig. 1. SRT parameters measured using calibrators at the bands of 92 cm (a) and 18 cm (b) in 2011−2013. Channel 1 (ch1) corresponds to receiving left circular polarization, channel 2 (ch2) to right.

bands, except 92 cm, are installed in open space on a cold plate cooled to a temperature of 130 K by radiation. Each receiver consists of two identical channels on which the input from the antenna through the antenna-feed assembly (AFA) with polarization splitter, radiation arrives in the left and right circular polarizations. Each channel has two parallel outputs, i.e., (1) a radiometric output with the detected signal, which arrives at the spacecraft telemetry system and is used in the antenna measurements, and (2) an interferometric output with a signal at intermediate frequency, which, after subsequent transformation, is used in the ground−space interferometer operation.

Special sessions of observations of calibration objects were usually carried out in the mode of the single telescope operation. Then, after buffer recording and storing in the onboard memory, the telemetry data were transmitted to the Earth during the day via the narrow-beam antenna by the service spacecraft telemetry radio channel. When interferometric observing researched sources the telemetry system data are sequentially placed in the headers of each frame of the data stream for the interferometer and transmitted online to the Earth through the narrow-beam antenna with the diameter of 1.5 m via the scientific high-data-rate radio channel. This makes it possible to allocate the telemetered radiometric signal from the interferometric data stream from SRT. In this manner, in this work, the results of the antenna measurements were obtained for sources studied with the interferometer in the scientific programs. The results of all measurements and analysis are summarized in Figs. 1−3 and Table 1−4.

2. DISCUSSION OF MEASUREMENTS

2.1. The 92-, 18-, 6.2-, and 1.35-cm Bands

A measurement analysis shows that almost all basic antenna parameters vary from measurement to measurement. We associate the main reason for these variations with variations in the temperature conditions of the antenna−feeder tract and the receiver. Physical temperatures of the elements of antenna−feeder tract and LNA on the cold plate can vary due to variations in the angle between the directions to the Sun and the measurement object from session to session. The closer the angle to the design boundary ($\approx 110°$) of the permitted SRT operation, the larger the expected deviations of the physical and noise temperature from their average values. In this case, the contribution to the equivalent noise temperature of the system should be varied versus the losses in the antenna feeds with polarization splitters. Therefore, significant variations in the noise equivalent temperature T_{NS} of the calibration signal should also be expected. This signal from the internal noise generator arrives at the receiver tract at the LNA input and is reduced to the recalculation of the telescope input through all elements of the antenna−feeder tract.

Therefore, to further simplify the analysis, the condition of the constancy of the mean values T_{NS} and the effective area A_{eff} was assumed to be fulfilled. Then, all of their real variations automatically refer to variations in T_{sys}. Note that this procedure does not affect the correctness of the astronomical calibration of the measurements using the parameter F_{sys} (SEFD) depending on the ratio of T_{sys}/A_{eff}. In this case, the results presented below for the mean-square deviations T_{sys} and F_{sys} for calibration and studied sources,
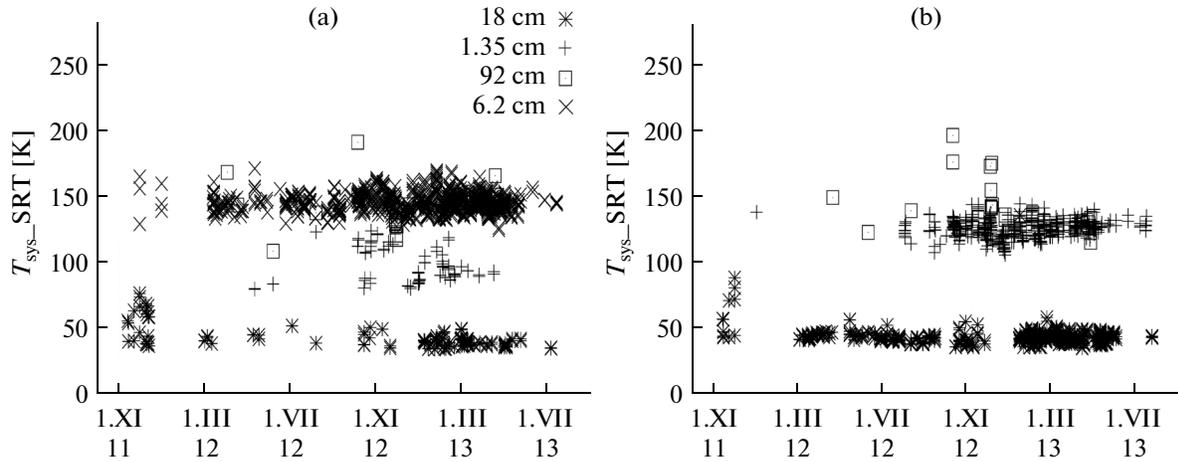
Fig. 2. SRT parameters measured using studied sources in 2011−2013: (a) channel 1 for right circular polarization at the band of 1.35 cm, left for remaining bands; (b) channel 2 for left circular polarization at the band of 1.35 cm, right circular polarization for the remaining bands.

which do not exceed approximately 13%, can be used to substantiate this condition.

Within the measurement errors, the obtained results for the mean values of the system temperature T_{sys} and the flux density F_{sys} (SEFD) at bands of 92, 18, 6.2, and 1.35 cm (Figs. 1, 2 and Tables 1, 2), taking into account the various contributions of sky background, which agree for both the calibration and researched sources, as well as with the first results presented in [5]: within (20−25)% at the band of 1.35 cm and (10−15)% at other bands. Approximately half of these values can be associated with slow systematic evolution of the parameters including their calibration.

A significant contribution to the observed spread of values T_{sys} relative to the mean can give variation of the LNA mismatch with the AFA−LNA input tract and variations associated with that of the LNA noise coefficient, which depend on the physical temperature of AFA and LNA (usually, there is no decoupling at the LNA input to reduce the noise temperature of the receiver).

2.2. The 18−25-GHz Band

The band is intended for use in the mode of the multifrequency interferometer synthesis and consists of the eight following subbands (with indicated central frequencies) spaced one after the other at 960 MHz [5]: F-4 (18 392 MHz), F-3 (19 352 MHz), F-2 (20 312 MHz), F-1 (21 272 MHz), F0 (22 232 MHz), F1 (23 192 MHz), F2 (24 152 MHz), F3 (25 112 MHz) (Fig. 3). Values of the center frequencies may be 4 MHz more or less than indicated depending on the given mode of operation of the scientific equipment. The measurement results of F_{sys} (SEFD$_{SRT}$) in these subbands shown in Fig. 3, and the estimate of the interferometer sensitivity in Table 3 confirm the theoretically expected monotonous "course" of SEFD$_{SRT}$

and the interferometer sensitivity with increasing frequency except, perhaps, of their behavior at the extreme frequencies, near 18 and 25 GHz. The sensitivities given in Table 3 are calculated according the known formula [5]

$$\sigma_{GBT\text{-}SRT} = b\sqrt{\frac{SEFD_{GBT}SEFD_{SRT}}{2\Delta\nu_{IF}\Delta t}}, \qquad (1)$$
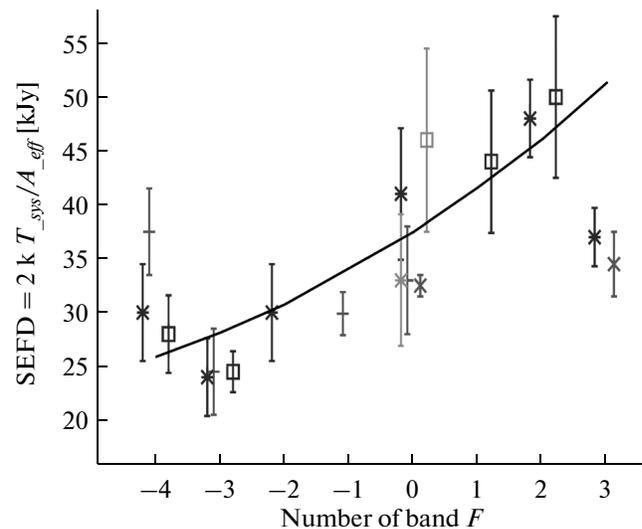

Fig. 3. Results of measurements of the SRT system equivalent flux density (SEFD) for eight subbands from F-4 to F-3 at frequencies from 18.4 to 25.1 GHz for the 3C 84 galaxy in 2011−2012. Signs with measurement errors are the data for channel 1 (right circular polarization) at the left of vertical line with the number of band F and for channel 2 (left circular polarization) at the right. Solid curve is the calculated estimate in the model of phase distortion.

Table 1. Results of mass measurements (rows 1.1-2.2) and calculated estimations (rows 3.1-3.12) when observing the calibration and studied sources in the left (LCP) and right (RCP) circular polarizations in 2011−2013

Parameter	1.35 cm	6.2 cm	18 cm	92 cm
	LCP; RCP	LCP; RCP	LCP; RCP	LCP; RCP
1. Calibrators				
1.1. T_{sys}, K	98 ± 13; 82 ± 11	133 ± 17; −	47.2 ± 1.0; 48.4 ± 1.0	230 ± 5; 210 ± 11
1.2. F_{sys}, kJy	36.0 ± 3.6; 30 ± 3.0	10.5 ± 1.1; −	3.18 ± 0.06; 3.26 ± 0.07	21.2±0.42; 19.4±1.0
2. Other objects				
2.1. T_{sys}, K	127 ± 8; 100 ± 10	147 ± 8; −	41.0 ± 1.0; 43.5 ± 4.0	145 ± 15; 147 ± 15
2.2. F_{sys}, kJy	46.7 ± 3.0; 36.8 ± 3.7	11.6 ± 0.6; −	2.76 ± 0.27; 2.93 ± 0.27	13.3 ± 1.4; 13.5 ± 1.4
3. Calculation of T_{sys} and F_{sys}				
3.1. Transmission coefficient:				
− Cable K_3/t_3	0.99/157	0.94/157	0.95/157	0.98/233
− AFA K_2/t_2	0.76; 0.84/175	0.68/175	0.95/175	0.83/175
− Antenna K_1/t_1	0.98/200	0.98/200	0.98/200	0.98/200
3.2. T_{rec}/t_4, K	45/140	26/140	15/140	39/290
3.3. ΔT_{rec}, K	61; 55	42	17	49
3.4. ΔT_{cable}, K	2	15	8.9	6
3.5. ΔT_{AFA}, K	56; 34	84	9.4	36
3.6. ΔT_A, K	4	4	4	4
3.7. T_{sky}, K	3	3	3	3 + 50
3.8. T_{sys}, K	126; 98	148	42.3	98 + 50
3.9. F_{sys}, kJy	46.4; 36.1	11.7	2.85	13.6
Calibrators:				
3.10. T_{sky}, K	−	−	3 + 5	3 + 120
3.11. T_{sys}, K	−	−	42.3 + 5	98 + 120
3.12. F_{sys}, kJy	−	−	3.18	19.5

Measurements of calibrators at the bands of 1.35 and 6.2 cm are given for 2011−2012. Errors of the scale of spectral flux density are not included. In rows 3.3−3.6 and 3.7 (3.10), we present estimates of contributions in T_{sys} from noise temperatures of receiver T_{rec}, cable (waveguide at the band of 1.35 cm) T_{cable}, antenna-feed assembly T_{AFA}, antenna T_A, and sky background T_{sky}, respectively.

where $b = 1/0.637$, $SEFD_{GBT} = 23$ Jy (for the HPAO radio telescope at Green Bank), $\Delta v_{IF} = 16$ MHz is the band of recorded frequencies, $\Delta t = 5$ min is the time of signal integration. Depending on the operating mode of the interferometer, signal recording is also possible at the band $\Delta v_{IF} = 32$ MHz [5]. The value $\Delta v_{IF} = 16$ MHz is used for uniformity with [6].

Based on the data in Fig. 3 and Table 3, it is possible to take interferometric measurements at five longwave subbands from F-4 to F0 with asensitivity of no lower than in F0 at a frequency of 22 GHz (with a wavelength of 1.35 cm). At three short-wave subbands F1, F2, and F3, the sensitivity can be lower than in F0 by a factor of 1.5 because of the strong contribution of the phase errors at wavelengths less than 1.35 cm. This

wavelength is close to the so-called minimum design wavelength of the telescope use $\lambda_{min} \equiv (16−20)\sigma \approx 18\sigma = 1.39$ cm at the design value $\sigma = 0.77$ mm (for details, see [5, 8−10] and chapters 3.2 and 3.3 further).

3. NUMERICAL INTERPRETATION OF THE MEASUREMENTS RESULTS

3.1. Equivalent Noise Temperature of SRT System T_{sys}

To explain the measured values T_{sys}, we numerically estimate the parameters of the antenna, antenna−feeder system, and receivers that affect T_{sys}. Usually, the SRT system in each of the polarization channels can be represented as a block diagram of four

Table 2. Basic SRT parameters according to [5] and mass measurements of F_{sys} and T_{sys} in the left (LCP) and right (RCP) circular polarizations in 2011−2013

Parameter	1.35 cm	6.2 cm	18 cm	92 cm
	LCP; RCP	LCP; RCP	LCP; RCP	LCP; RCP
SRT in flight, 2011−2013:				
1. $(\vartheta_{0.5} \pm 5\%) \cdot (\varphi_{0.5} \pm 5\%)$	$6.0' \times 13'$	$25'$	$72'$	$6°.1$
2. $A_{eff} \pm 10\%$, m^2	7.5	35	41	30
3. AE $= A_{eff}/A_{geom} \pm 10\%$	0.1	0.45	0.52	0.38
4. $T_{sys} \pm 13\%$	127; 100	147; −	41.0; 43.5	145; 147
5. $F_{sys} \pm 10\%$ (SEFD), kJy	46.7; 36.8	11.6; −	2.76; 2.93	13.3; 13.5
6. Amplification, Jy/K	368	78.9	67.3	92.0
7. $\Delta\vartheta_S$	$-1.2' \pm 0.2'$			
8. $\Delta\varphi_S$	$<1.5'$			
9. $\Delta\varphi_P$	$2.5'$			
10. σ_{SVLBI}, mJy (at $\Delta t = 5$ min; $\Delta\nu = 16$ MHz)	17; 15	5; −	3; 3	14; 14
11. $\alpha_D = (\vartheta_{0.5} \cdot \varphi_{0.5})\, D/\lambda$	1.29×2.80	1.17	1.16	1.16

In rows 1−11, we present the width of the main lobe of the radiation pattern at half power (1); the effective area (2); aperture efficiency (3); system equivalent noise temperature (4); system equivalent flux density (5); telescope amplification (6); systematic error when scanning the sky area over two coordinates (7) and (8) after entering constant correction (9) in pointing the telescope; sensitivity of the interferometer SRT-Green Bank Telescope by (1) and [6] (10); the ratio of measured width to ideal width λ/D of the main lobe of the radiation pattern (11).

sequential units [5], i.e., (*1*) an antenna, (*2*) an antenna-feed assembly (AFA) with an input polarization splitter on the left and right circular), (*3*) a VHF-cable/waveguide that connects units (*2*) and (*4*), and (*4*) a receiver with input a low-noise amplifier (LNA). Then, the equivalent noise temperature T_{sys} reduced to the input of this system can be written as follows:

$$T_{sys} = T_{sky} + T_1 + T_2 L_1 + T_3 L_1 L_2 + T_4 L_1 L_2 L_3, \quad (2)$$

$$T_i = t_i(L_i - 1), \; L_i \equiv 1/K_i, \; i = 1, 2, 3. \quad (3)$$

Here, T_{sky} is the antenna temperature of the sky at the antenna input; T_i is equivalent noise temperatures of four units reduced to the input of own unit, including the antenna ($i = 1$), AFA ($i = 2$), cable ($i = 3$), and receiver ($i = 4$); and t_i, L_i, and K_i are the physical temperature and coefficients of losses and power transmission for ith unit, respectively. Each summand in (2) reduces (recounts) the unit noise temperature to the antenna input, i.e., to the input of the entire SRT system and, thus, allows one to estimate the contribution of the corresponding unit in the complete noise temperature of the radio telescope system. In this case, to simplify it is assumed that the losses L_i have only

active component, and all units are perfectly matched with each other.

Note that AFA contributes to three out of five summands in (2) (due to difference of $L_2 = 1/K_2$ from the ideal case of the absence of losses, when L_2 is equal to

Table 3. Estimate of sensitivity $\sigma_{GBT\text{-}SRT}$ of the interferometer SRT−Green Bank Telescope for 8 subbands

Band	Frequency, GHz	SEFD$_{SRT}$, kJy	$1\sigma_{GBT\text{-}SRT}$, mJy
1. *F*-4	18.392	26	12
2. *F*-3	19.352	28	13
3. *F*-2	20.312	31	14
4. *F*-1	21.272	34	14
5. *F*0	22.232	37	15
6. *F*1	23.192	41	16
7. *F*2	24.152	46	16
8. *F*3	25.112	51	17

Table 4. Typical values of losses, AE, and A_{eff} estimated by the method for reflectory antennas [8]

Parameter	1.35 cm	6.2 cm	18 cm
1. $A_{eff} = AEA_{geom}$, m^2	21	36	39
2. AE $= \eta_1\eta_2\eta_4\eta_7\eta_9\eta_{10}\eta_{12}$	0.28	0.46	0.50
2.1. η_1 (losses at reflection)	0.96	0.96	0.96
2.2. η_2 (at absorption)	0.85	0.85	0.90
2.3. η_4 (at overradiation)	0.834	0.834	0.834
2.4. η_7 (at rms mirror error)	0.598	0.976	0.997
2.5. η_9 (at shading from AFA)	0.96	0.96	0.96
2.6. η_{10} (at scattering on four rods)	0.935	0.935	0.935
2.7. η_{12} (at radiation nonuniformity)	0.773	0.773	0.773

one). Therefore, losses in AFA are the most considerable losses when forming the overall noise telescope temperature. Lower values of L_2 are obtained when the matching calculated and measured noise telescope temperatures are close, (within approximately 10%) to typical values in ground feeds of this type and caused by the compactness and coaxiality of feeds, as well as their association with polarization splitters in united four-frequency unit. Additional losses in AFA at the band of 1.35 cm can occur when formed and propagated in higher types of waveguide modes due to the increased diameter of the circular input waveguide (to provide the requirement for feed operation in the extended frequency band at 18−25 GHz needed to synthesize the interferometric mode of the frequency).

Usually, the physical temperature in the real sessions of radio-astronomy observations with SRT were supported by the thermal control system within $t_4 = 130-150$ K for LNA on the cold plate and $t_2 = 150-200$ K for AFA using radiative cooling of the cold plate. For numerical estimates of the values in (2) and (3), for all bands, we take the following: $t_4 = 140$ K ($t_4 = 290$ K for the band of 92 cm), $t_2 = 175$ K, $t_3 = (t_2 + t_4)/2$, $t_1 = 200$ K, $T_{sky} = 3$ K, and $K_1 = 0.98$ (the design value). Then, for these values and the values of other parameters, depending on the band, as discussed below, we obtain estimates of T_{sys} and the corresponding contributions from the receiver, elements of antenna−feeder tract, and sky background, which are summarized in Table 1.

3.1.1. The 92-cm Band

T_{sys} ($K_2 = 0.83$; $K_3 = 0.98$; $T_4 = 39$ K) $= 3 + 4 + 36 + 6 + 49 = 98$ K. Here and below, five numerical summands correspond to the contributions from the five summands in (2). It can be seen from here that the

main contribution to the system temperature without the Galactic background makes contributions from AFA (third summand, 36 K) and LNA (fifth summand, 49 K). Assuming that the difference of the measured system temperature (Table 1) and this one is mainly determined by anisotropic radiation of the Galactic background, we obtain $T_{sky} \approx 50$ K; $T_{sys} \approx 150$ K for the researched sources in the interferometric sessions; and $T_{sky} \approx 120$ K, $T_{sys} \approx 220$ K for calibrators. To test this hypothesis, a detailed analysis is required that takes into account the individual observational conditions.

3.1.2. The 18-cm Band

T_{sys} ($K_2 = 0.95$; $K_3 = 0.95$; $T_4 = 15$ K) $= 3 + 4 + 9.4 + 8.9 + 17 = 42.3$ K. Due to the relatively low losses, the LNA noise, cables, and AFA (summands from fifth to third) make the main contributions. The small difference between measured T_{sys} when observing calibrators and other objects can be referred to the corresponding background excess near the Galactic plane because the most studied sources are extragalactic.

3.1.3. The 6.2-cm Band

T_{sys} ($K_2 = 0.68$; $K_3 = 0.94$; $T_4 = 26$ K) $= 3 + 4 + 84 + 15 + 42 = 148$ K. It was noted in [5] that, in this band, there is an approximately twofold excess of the measured noise temperature over the expected value. It can be seen that the measured value can be formally explained by increasing active losses in AFA over the design. The measurements for calibrators and other objects coincide within errors. However, taking into account that the stable operation in flight was found to only be possible at separate operation with channels of left and right polarizations (otherwise both channels were in the off-scale level due to the self-excitation of one or both channels [5]), a mechanism is also possi-

ble at which, because of the temperature sensitivity of the LNA and AFA characteristics (with polarization splitters) when cooling from 300 to 130−150 K, during flight, the coordination of LNA and AFA with the tract worsened and reactive losses and LNA noise coefficient increased such that the operating conditions of one or both channels were found to be close to the conditions of self-excitation. However, the operation with channels was still individually stable.

3.1.4. The 1.35-cm Band

T_{sys} ($K_2 = 0.84$; $K_3 = 0.99$; $T_4 = 45$ K) $= 3 + 4 + 34 + 2 + 55 = 98$ K is for channel 1. T_{sys} ($K_2 = 0.76$; $K_3 = 0.99$; $T_4 = 45$ K) $= 3 + 4 + 56 + 2 + 61 = 126$ K is for channel 2. As before, to explain the average measured values T_{sys}, it is sufficient to admit the presence of active losses in AFA with the average values of the AFA transmission coefficient indicated here and in Table 1 with other variables that affect T_{sys} being fixed. In the general case, the reactive losses, variations in the LNA noise coefficient and increases the active losses $L_3 = 1/K_3$ due to a reduced conductivity of the coating of waveguide walls over time should also be taken into account. The spread of individual measurements relative to the average is naturally obtained by varying physical and noise temperatures, as well as other parameters that enter into ratios (2)−(3). Individual variations in these parameters depend on the physical temperature of the elements of the antenna−feeder tract, i.e., on the conditions of temperature control, and, therefore, are primarily determined by variations in the orientation of the space radio telescope relative to the Sun in individual observational sessions. The difference in the measured average values F_{sys} and T_{sys} for calibrators and other objects (about 20−25%, see Table 1), except for measurement errors, can include the effect of different temperature conditions for observations of these objects on average.

3.2. Effective Area and Radiation Pattern

The effective area A_{eff} at wavelength λ is associated with so-called effective solid angles Ω_A of the antenna radiation pattern, Ω_{beam} of main lobe of the radiation pattern, and Ω_{lobe} outside the main lobe by known ratios as follows:

$$\Omega_A = \int_{4\pi} D(\theta, \varphi)d\omega = \Omega_{beam} + \Omega_{lobe} = \lambda^2/A_{eff}, \quad (4)$$

$$\Omega_{beam} = \int_{\varpi_{beam}} D(\theta, \varphi)d\omega \approx k_0\vartheta_{0.5}\varphi_{0/5}, \quad (5)$$

$$\Omega_{lobe} = \int_{\varpi_{lobe}} D(\theta, \varphi)d\omega, \quad (6)$$

$$\frac{\Omega_{beam}}{\Omega_A} + \frac{\Omega_{lobe}}{\Omega_A} = 1. \quad (7)$$

In (4), (5), and (6), the radiation pattern $D(\vartheta, \varphi)$ is integrated over solid angles within 4π, of the main lobe and outside the main lobe, respectively, $\omega_{lobe} = 4\pi - \omega_{beam}$; $\vartheta_{0.5}$ and $\varphi_{0.5}$ is main lobe width at half power for mutually perpendicular directions ϑ and φ, and the coefficient $k_0 = 1-1.15$ depends on the shape of mirror irradiation ($k_0 = 1$ at the uniform distribution of the electric field over the aperture, $k_0 = 1.13$ at the Gaussian distribution [7]). The first summand in (7) is usually designated as the coefficient of radiation pattern using and the second is designated as the coefficient of radiation scattering outside the main lobe.

One should note the rather common mistake even among specialists according to which the measurements of the main lobe can supposedly yield the value of the effective area. In fact, from (4)−(7), the only correct conclusion is that, without knowing information on the portion of radiation dissipated by the antenna in the effective solid angle Ω_{lobe} (as in this case), it is not possible to do this correctly.

We estimate values of the SRT effective area, which can be expected for typical accepted phase errors in the antenna−feeder system. For this, we consider the aperture efficiency AE $= A_{eff}/A_{geom}$, where A_{eff} and $A_{geom} = 75.8$ m^2 are effective and geometric areas of the SRT mirror aperture, respectively, and we use the AE representation through seven main of twelve usually used coefficients [7, 8], each of which describes one of the typical causes of area losses for reflector antennas (see rows 2.1−2.7 in Table 4; we assume that the remaining five coefficients are equal to 1).

Comparing the obtained typical estimates of the effective area and AE shown in Table 4 with the results of measurements (Table 2), it is seen a good agreement for the bands of 6.2 and 18 cm. The difference between the typical design value of 21 m^2 and the measured value at the band of 1.35 cm is connected with additional phase errors in the mirror aperture, an analysis of possible causes of which is presented in our paper [5] and will be continued below. The typical AE estimate for the band of 92 cm was not carried out, since the ratio of wavelength to the diameter of the mirror is not low enough for the correctness of using values of the typical coefficients, and the reliability of this estimation does not seem high.

Flight tests of the RadioAstron telescope [4, 5] showed agreement between the basic measured characteristics with the design characteristics at the bands of 92 and 18 cm and their difference from the design characteristics for the equivalent noise temperature of the system at the band of 6.2 cm and for a width of the main lobe and the effective area at the band of 1.35 cm. At the minimum wavelength of 1.35 cm of design using the space radio telescope the main lobe of the radiation pattern was found to be considerably asymmetric (wider by a factor of 2 than the design value in one of the mutually orthogonal sections) that indicated to the

corresponding errors of the phase distribution of the field in the antenna aperture. As a consequence, these phase errors led to a decrease in the effective area and, as a result, to an increase in SEFD and a decrease in the SRT and interferometer sensitivities [5]. Further measurements and analysis, on which we will report in this paper, confirm these results.

3.3. Model of Phase Distortions

One possible reason for these phase distortions is considered in [5], i.e., the system astigmatism due to the features of the phase feed radiation pattern. Another reason is estimated here as follows: astigmatism caused by a slight variation in the SRT mirror shape, which in the first approximation transforms the parabolic mirror with the circular aperture of diameter D and focal length F into a slightly elliptical aperture with the principal axes of the ellipse D_1 and D_2 close to D, and corresponding centers of focusing F_1 and F_2 in mutually orthogonal sections. This deformation of the mirror shape seems possible if residual stresses in tension for rods to 27 hard mirror lobes are various and exceeds the design characteristics. It can be expected that stronger tension leads to smaller profiles of the quasiparabolic surface in the corresponding sections of the mirror with a shift in the centers of focusing in the directions from the mirror.

To simplify the numerical estimates in any sections that contain the mirror axis, we propose to maintain the axis position and the parabolic profile of the cross section with the design ratio $a = F/D$. Then, the variations in the aperture size in this cross section from D to $D_1(D_2)$ leads to a mismatch of the focus F with $F_1(F_2)$ in this cross section, i.e., to astigmatism of the mirror, and the feed fixedly installed on the Earth on the calculated focus F is found to be shifted in flight relative to F_1 and/or F_2 that for the system of 27 lobes give the total phase errors in the aperture and the broadening of the telescope radiation pattern. Let us consider this effect quantitatively using the results of Kuhn's monograph [9] in order to associate the maximum quadratic phase error Φ at the edge of the parabolic mirror with the feed shift δ from focus along the focal axis at wavelength λ:

$$\Phi = 4\pi \frac{\delta}{\lambda} \frac{1}{1 + (4a)^2}. \qquad (8)$$

According to [5], in (8), we assume that $\Phi \approx 1.5\pi$, $\lambda = 1.35$ cm, $a = 0.43$ (the design value for SRT), as well as taking into account for this case $\delta = \Delta F = a\Delta D$, $\Delta F \equiv F_1 - F_2$, $\Delta D \equiv D_1 - D_2$, $D_2 = 10$ m, we obtain $\delta \approx 2.0$ cm, $\Delta D = \delta/a \approx 2.0/0.43 \approx 4.7$ cm and the eccentricity E of the ellipse $E = D_1/D_2 \approx 10.047/10 \approx 1.0047$. Thus, under these assumptions, a small deformation of the SRT mirror shape that transforms the circular aperture with a diameter of 10 m into elliptical with eccentricity $E \approx 1.0047$ (the major axes of the

ellipse are equal to about 10 m and 10.047 m), can cause astigmatism of the mirror that leads to the observed features of the measurement results of the SRT characteristics at the band of 1.35 cm.

In eight subbands, for the mode of frequency synthesis, we can expect smooth variations in the shape of the main lobe of the radiation pattern and the telescope effective area that correspond to variations of phase error (8) from $\Phi \approx 1.1\pi$ to $\Phi \approx 1.6\pi$ at the frequencies of 18–25 GHz. For the remaining standard bands of SRT ($\lambda \geq 6.2$ cm), the phase error (8) is the value $\Phi \leq \pi/3.3$ close to $\Phi \leq \pi/4$, which is generally considered to be the permissible phase error.

Let us numerically estimate the influence of phase errors in the antenna–feeder system to variations in the effective area A_{eff} at frequencies of 18–25 GHz. In this case, using typical values of the area equal to 21 m², according to Table 4 and the product of three coefficients $k_1(\lambda)$, $k_2(\lambda)$, and $k_3(\lambda)$, we perform the following: $A_{\text{eff}}/A_0 = k_1(\lambda)k_2(\lambda)k_3$. Here, $A_0 = 21/\eta_7 = 35$ m² corresponds to a typical effective area in the total absence of phase distortions ($\eta_7 = 0.598$ from Table 4); $k_1(\lambda) = \exp[-(4\pi\sigma/\lambda)^2]$ [8] takes into account the known contribution from random phase errors at the root-mean-square deviation σ of the mirror surface profile from the ideal parabolic mirror ($k_1(\lambda) = \eta_7 = 0.598$ at $\lambda = 1.35$ cm, $\sigma = 0.77$ mm); $k_2 = [\eta(\varphi = 0)\eta(\varphi = \Phi)]^{1/2}$ at $\eta(\varphi) = 6.55(1.01 - 0.2\cos\varphi)/(5.3 + \varphi^2)$ [10] gives an estimate of the contribution from the effects considered above with quadratic phase error (8) of the mirror. Here, $k_3 \approx 0.73$ is taken as the value of the contribution from the phase error of mirror irradiation, including the difference of the AFA phase radiation pattern from ideal (see in detail [5, 8, 10]).

Then, at $\lambda = 1.35$ cm, $T_{\text{sys}} = \text{const} = 100$ K, the design value $\sigma = 0.77$ mm, $\Phi \approx 1.5\pi$, we obtain $k_2(\lambda) = 0.49$, $A_{\text{eff}} = 21k_2(\lambda)k_3$ m² = 7.5 m², $SEFD_{\text{SRT}} = 37$ kJy and numerical dependence of $SEFD_{\text{SRT}}$ on the frequency, which is shown in Fig. 3 by a solid line. It can be seen that the calculated estimate agrees with the measurements for all subbands except extreme within accuracy. The deviations of calculated values relative to those measured at the extreme frequencies near 18 and 25 GHz can be explained by the violation of the assumption $T_{\text{sys}} = \text{const}$ in these subbands. The corresponding estimates of the expected interferometer sensitivity for eight subbands are shown in Table 3.

Thus, the results of the antenna measurements in eight subbands at frequencies of 18 to 25 GHz (the noise temperature of the system, the effective area, the system equivalent flux density (SEFD), and their dependence on the frequency) can be concordantly explained in the model of phase distortion developing the model considered in [5].

According to our estimates of loss coefficients (see Table 4) by the known method [8], the typical effective area at the band of 1.35 cm should be close to 35 m² at the absence of any phase distortions and to 21 m² at the presence of only design phase losses k_1 of the area

due to the random errors of the mirror surface; in this case, the aperture efficiency is about 0.45 and 0.27, respectively.

In the model, coefficient $k_2 \approx 0.49$ reduces the typical design area of 21 m^2 by a factor of two due to astigmatism and the quadratic phase error of the mirror surface, assuming that the circular aperture of the mirror with diameter of 10 m was the quasi-elliptic with the principal axes of 10 m and 10.047 m, and the coefficient $k_3 \approx 0.73$ decrease further by a factor of about 1.5 due to the phase distortions of mirror irradiation similar to [5]. As a result, the effective area of 35 m^2 (at $\eta_7 = k_1 = k_2 = k_3 = 1$) or 21 m^2 (at $\eta_7 = k_1 = 0.598$) decreases to the measured value $A_{\text{eff}} \approx 7.5$ m^2, and an asymmetry of the main lobe of the radiation pattern arises due to the system astigmatism and the total phase errors in the antenna aperture.

Similar phase errors and losses in the antenna–feeder system distorting the radiation pattern and reducing the effective area, the cases of the self-excitation of the receiver are a typical, well-known situation for ground-based telescopes, especially at the beginning of operation at short wavelengths close to the minimum wavelength of the telescope operation. The reasons for these effects are usually partially excluded by additional surface adjustment and correction of mirror exposure, corrections of focusing, debugging or replacing elements of the antenna–feeder system and the receiver, and improving their coordination with each other.

Formally, in the discussed model, it is possible to reduce astigmatism caused by the deviation of the parabolic mirror shape from design by reducing the residual forces of lobe tension through the cable and a rod of mirror opening mechanism using commands from the Earth. However, the utility of this operation is questionable up to finishing observations on the main priority scientific goals.

The main reasons for doubt are as follows:

(1) upon failure, there is no guarantee that the antenna will be returned to the previous position;

(2) we must perform new labor-intensive antenna measurements;

(3) a gain in the effective area can be accompanied by losses, e.g., in pointing the antenna, which today are nearly absent, also because of the broadening of the main lobe of the radiation pattern.

New inevitable errors can partially or completely compensate for expected improvements at the band of 1.35 cm, i.e., increasing the SRT effective area up to a factor of two (due to variations of k_2 from 0.5 to 1) and the interferometer sensitivity up to a factor of 1.5 according to (1).

CONCLUSIONS

New results of the radiometric measurements of the space radio telescope parameters in 2011–2013

using the calibration objects with the single SRT and a large number of the researched sources in the interferometer mode agree with the first results obtained by Kardashev et al. [5] within 10–15% at the bands of 92, 18, and 6.2 cm and 20–25% at the band of 1.35 cm.

The main contribution to SEFD and the SRT sensitivity at the bands of 92, 18, and 6.2 cm make noise of the receiver and antenna feed unit and, at the band of 1.35 cm, makes losses of the effective area due to phase errors in the antenna–feeder system. The SRT contribution in the sensitivity of the ground–space interferometer proportional to the square root of measured values SEFD is close to the design at the bands of 92 and 18 cm, and reduces the design sensitivity approximately by a factor of 1.5 and 2 at the bands of 6.2 and 1.35 cm, respectively. The measured SRT contribution increases the sensitivity of the interferometer to a factor of up to 1.5 in five subbands at frequencies of 22–18 GHz and reduces it by a factor of 1.5 in three subbands at frequencies of 22–25 GHz relative to the sensitivity at 22 GHz.

The main contribution to the SRT equivalent noise temperature makes the receiver and the antenna-feed assembly (AFA) with polarization splitters. The spread in values of the noise temperature through the dependence on the physical temperature of LNA and AFA can be associated with the variations in the SRT orientation relative to the Sun in individual observational sessions.

The obtained results and SRT operating experience can be useful when designing future space projects (Millimetron, etc.), especially taking into account that the SRT antenna is probably the largest construction project to date opening in space. These results indicate the need to optimize the design of the phase errors of the surface and the mirror exposure and minimize the losses in both individual elements and the antenna–feeder system with the receiver as a whole. To reduce the phase distortion near the minimum wavelength of the telescope operation it can be appropriate the additional design lack of irradiation of the mirror edge reducing known optimum level by several times.

REFERENCES

1. Khartov, V.V., A new stage in the development of robotic spacecraft for fundamental space research, *Solar System Research*, 2012, vol. 46, pp. 451–457.

2. Kardashev, N.S., Aleksandrov, Yu.A., Andreyanov, V.V., et al., RadioAstron (the *Spektr-R* project): A radio telescope much larger than the Earth. Basic parameters and tests, *Solar Systen Research*, 2012, vol. 46, pp. 458–465.

3. Kardashev, N.S., Aleksandrov, Yu.A., Andreyanov, V.V., et al., RadioAstron (the *Spektr-R* project): A radio telescope much larger than the Earth. Ground segment and key science areas, *Solar System Research*, 2012, vol. 46, pp. 466-475.

4. Avdeev, V.Yu., Alakoz, A.V., Aleksandrov, Yu.A., et al., The *RadioAstron* space mission. First results, *Vestnik FGUP NPO im. S.A. Lavochkina*, 2012, no. 3, pp. 4–21.

5. Kardashev, N.S., Khartov, V.V., Abramov, V.V., et al., RadioAstron— A telescope with a size of 300000 km: main parameters and first observational results, *Astronomy Reports*, 2013, vol. 57, pp. 153–194.

6. *RadioAstron User Handbook*. http://www.asc.rssi.ru/radioastron/documents/rauh/en/rauh.pdf

7. Kraus, J.D., *Radio Astronomy*, McGraw-Hill, 1966. Translated under the title *Radioastronomiya*, Moscow: Sov. Radio, 1973.

8. Esepkina, N.A., Korol'kov, D.V., and Pariiskii, Yu.N., *Radioteleskopy i radiometry* (Radio Telescopes and Radiometry), Moscow: Nauka, 1973.

9. Kühn, R., *Mikrowellenantennen*, Berlin: Veb Verlag Technik, 1964. Translated under the title *Mikrovolnovye antenny*, Moscow: Sudostroenie, 1967.

10. Tseitlin, A.M., *Antennaya tekhnika i radioastronomiya* (Antenna Technology and Radio Astronomy), Moscow: Sov. Radio, 1976.

Translated by N. Topchiev